Research Square

Preprints are preliminary reports that have not undergone peer review. They should not be considered conclusive, used to inform clinical practice, or referenced by the media as validated information.

Near 14 cm2 V-1 s-1 Charge Carrier Mobility Enabled by Amorphous Indacenodithiophene-based Polymers with Controlled Regioregularity

Yongjoon Cho
Ulsan National Institute of Science and Technology
Sohee Park
Ewha Womans University
Seonghun Jeong
Ulsan National Institute of Science and Technology
Heesoo Yang
Ewha Womans University
Byongkyu Lee
Ulsan National Institute of Science and Technology
Sang Myeon Lee
Ulsan National Institute of Science and Technology
Byoung Lee
Ewha Womans University
Changduk Yang (yang@unist.ac.kr)
Ulsan National Institute of Science and Technology https://orcid.org/0000-0001-7452-4681

Article

Keywords: Donor-accepted Polymers, Hole Mobilities, Semicrystalline Semiconductors, Stretchable Electronics

Posted Date: October 1st, 2020

DOI: https://doi.org/10.21203/rs.3.rs-78573/v1

License: This work is licensed under a Creative Commons Attribution 4.0 International License. Read Full License

Abstract

Herein, we report the synthesis and characterization of four regioregular, well-defined donor–acceptor polymers (P1, P2, P3, and P4), comprising different compositions of axisymmetric cyclopentadithiophene (CDT) and centrosymmetric indacenodithiophene (IDT) donors in conjugation with the asymmetric 5-fluoro-2,1,3-benzothiadiazole acceptor that is precisely oriented in the regular pattern along the backbone. Morphological analyses of the above polymer series show that exclusive CDT donor-containing P1 is semicrystalline, whereas the others (IDT donor-containing ones) are near-amorphous in nature. Comparatively, IDT donor-containing polymers have superior hole mobilities; in particular, exclusive IDT donor-containing polymer P4 offers an ultra-high mobility of 13.82 $cm^2 V^{-1} s^{-1}$ at a channel length of 200 *μm*, which is comparable to the recently reported values for state-of-the-art semicrystalline semiconductors. In addition, the near-amorphous characteristics render the IDT donor-containing polymer films highly ductile and stretchable. Such superior features, which are associated with excellent charge transport and ductility, demonstrate a promising possibility for application in viable stretchable electronics.

Introduction

π-conjugated polymers have been extensively studied for their application in printing organic field-effect transistor (FET) arrays and circuits to realize low-cost, large-area, flexible, and even stretchable next-generation electronics that cannot be realized using traditional silicon technologies.[1–7] On the basis of the principle that charge carrier mobility is unambiguously linked to the degree of order in the packing, more than a decade of research has focused on increasing the crystallinity of π-conjugated polymers as a strategy for improving charge transport; this has reliably boosted mobility to exceed 10 $cm^2 V^{-1} s^{-1}$.[8–13] Three major design strategies exist for enforcing polymer crystallinity: (i) donor–acceptor architecture in the backbone induces a strong intramolecular charge transfer (ICT) effect as an attractive force between the donor and acceptor units, resulting in a more planar configuration that facilitates π-electron delocalization along the backbone;[14–17] (ii) the incorporation of fused aromatic building segments into the backbone generates a large π-orbital overlapping area, formulating large crystalline domains with only few disordered domain boundaries;[12, 18–21] and (iii) a precise regioregularity in the polymer repeating units realizes enhanced structural arrangement of the chains, thus promoting self-organization.[16, 22–24] As a successful example that integrates all of the abovementioned concepts for FET applications, Bazan et al. have reported a semicrystalline polymer with the donor–acceptor structure comprising cyclopentadithiophene (CDT) as the fused aromatic donor unit and 5-fluoro-2,1,3-benzothiadiazole (FBT) acceptor with the regioregular orientation of F atoms.[23]

Compared to the axisymmetric CDT unit, indacenodithiophene (IDT), which contains peripheral thiophene rings held in a rigid arrangement through a central phenyl ring, is recognized as part of the extended CDT analogue centrosymmetric structure. Interestingly, polymers based on the extended fused-ring IDT core display high FET mobilities with high backbone coplanarity despite the lack of long-range crystalline

order in the solid state.[2, 3, 25–28] This intriguing feature considerably differs from the abovementioned theory and provides a new molecular-design guideline for achieving high mobilities in near-amorphous polymers, thus facilitating the development of intrinsically stretchable semiconducting polymers toward next-generation electronics. Driven by their unique, yet different properties, many polymers based on CDT and IDT units have been incorporated into high-performance FETs and continue to be studied (see Fig. 1 and **Table S1**).[2, 14, 16, 23, 26, 28–36] However, there is no systematic comparison study between CDT and IDT polymer systems with backbone regioregularity in terms of optoelectronic and morphological properties.

Herein, we aim to synthesize and characterize four donor–acceptor regioregular polymers (P1, P2, P3, and P4) with varied compositions of CDT and IDT donor subunits in conjugation with the regularly arranged FBT acceptor along the backbone; then, we investigate their intrinsic properties including their optical property, energetics, morphology, molecular packing, and charge transport. Notably, we discovered that in addition to their higher ductility, as evidenced by the crack onset strain measurement, FETs prepared using IDT donor-containing near-amorphous polymers show higher mobilities than those of exclusive CDT donor-containing semicrystalline P1. In particular, P4 exhibited an unprecedentedly high hole mobility of up to 13.82 $cm^2 V^{-1} s^{-1}$ at a channel length of 200 *μm*. To the best of our knowledge, this is the highest mobility value among near-amorphous polymers reported to date.

Results And Discussion

Synthesis, Characterization, and Computational Analysis

Density functional theory (DFT, B3LYP/6-31G+**) was first performed to gain insight into the structural difference (*e.g.*, conjugation lengths, electrostatic potentials, and net dipole moments) between the axisymmetric CDT and centrosymmetric IDT units, as shown in Figs. 2a,b. Compared with three-rings-fused CDT (with an effective π-conjugated length of 9.80 Å and a net dipole moment of 1.75 D), the five-rings-fused IDT shows a larger effective π-conjugated length (15.47 Å) and zero net dipole moment. In addition, in cyclic voltammetry (CV) measurement, the oxidation potential (E_{oxi}) of IDT is higher than that of CDT (see Fig. 2c), evidencing the relatively weaker electron-donating nature of the IDT unit.[37, 38]

With theoretical understanding of the structural features of axisymmetric CDT vs. centrosymmetric IDT units, 7,7'-(4,4-dihexadecyl-4*H*-cyclopenta[1,2-*b*:5,4-*b'*]dithiophene-2,6-diyl)bis(4-bromo-5-fluorobenzo[*c*][1, 2, 5]thiadiazole) (**M2**) and 7,7'-(4,4,9,9-tetrahexadecyl-4,9-dihydro-*s*-indaceno[1,2-*b*:5,6-*b'*]dithiophene-2,7-diyl)bis(4-bromo-5-fluorobenzo[*c*][1, 2, 5]thiadiazole) (**M4**) were prepared as key symmetrical monomers by the Still coupling reaction of 4,7-dibromo-5-fluoro-2,1,3-benzothiadiazole (FBT-Br_2) with (4,4-dihexadecyl-4*H*-cyclopenta[1,2-*b*:5,4-*b'*]dithiophene-2,6-diyl)bis(trimethylstannane) (**M1**) and (4,4,9,9-tetrahexadecyl-4,9-dihydro-*s*-indaceno[1,2-*b*:5,6-*b'*]dithiophene-2,7-diyl)bis(trimethylstannane) (**M3**) in yields as high as ~ 70%. The structures and purities of the final monomers were clearly verified using various analytical technologies such as nuclear magnetic resonance (NMR) spectroscopy and elementary analysis (EA) (see the experimental procedure and **Figures S10–13**). Four regioregular polymers with the

FBT units facing the same regular pattern along the backbones yet different backbone compositions were synthesized from the corresponding monomers under the same conditions ($Ph(PPh_3)_4$ as the catalyst in *o*-xylene under microwave heating at 220°C), as shown in Scheme 1. P1 and P4 exclusively contain CDT and IDT donor units on the backbones and alternatingly arranged FBT counterparts as acceptor units. However, both P2 and P3 are based on alternating CDT and IDT units with a different F-atom configuration of FBT (F-atoms pointing toward CDT for the former and toward IDT for the latter, respectively).

As shown in Fig. 3 and **Figures S14–17**, in addition to the accurate peak area integrations, high-temperature ^{1}H NMR of the polymers reveals four proton peaks in the aromatic region (three signals from the terminal thiophenes of CDT and IDT moieties in the down-field region and one from the flanking benzene of the IDT unit in the most up-field region), except for P1 having only three peaks owing to the absence of an IDT unit on its backbone. Notably, the chemical shifts of thiophene protons are very sensitive to the F-atom pointing direction of FBT, whereas a similar chemical shift (~ 8.05 ppm) is observed for the proton peaks of FBT units, regardless of the flanking donor building subunits (CDT and IDT). Overall, these data can elucidate the polymer structures with regioregularity but different backbone compositions. In addition to their good solubility in various organic solvents, all polymers have similar number-average molecular weight (M_n) of 88.4–93.5 kDa and polydispersity index (PDI) of 1.3–1.8, as determined by high-temperature gel-permeation chromatography (HT-GPC, 100 °C), which can minimize the influence of molecular weights on their photophysical and optoelectronic properties.

The ultraviolet–visible (UV–Vis) absorption spectra of the polymers in chloroform solutions and thin films are shown in Figs. 4a,b and the detailed relevant data are summarized in Table 1. All polymers have π–π* transition bands that are centered at approximately 410 nm and broad ICT transition bands ranging from 450 to 1000 nm. Notably, upon transitioning from solution to thin films, slight red-shifts occur for IDT donor-containing polymers (P2, P3, and P4), whereas no distinct absorption difference is observed for exclusive CDT donor-based P1. This suggests a breakup of the solid-state structural order within polymer chains to some extent with the incorporation of centrosymmetric IDT into the backbone.[30, 39] In addition, one can observe that absorption spectra shift toward longer wavelengths with increasing CDT content in the repeating polymer unit. Therefore, optical bandgaps (E_g^{opt}) determined by the onsets of absorptions in the films are in the order of P1 < P2 ≅ P3 < P4, indicating that CDT is a stronger electron donor relative to IDT; this result is consistent with the abovementioned CV-derived oxidation potentials.

Table 1
Optical and electrophysical properties of the Polymers.

	λ_{sol}^{max} [nm]	λ_{film}^{max} [nm]	λ_{onset} [nm]	E_g^{opt} [eV]	E_g^{CV} [eV]	E_{HOMO} [eV]	E_{LUMO} [eV]	Mn [kDa]	PDI
P1	433, 785	434, 786	948.6	1.31	1.67	-4.93	-3.26	88.4	1.31
P2	415, 693	424, 716	788.5	1.58	1.82	-5.17	-3.35	90.3	1.43
P3	418, 696	423, 719	791.2	1.57	1.82	-5.20	-3.38	84.0	1.50
P4	418, 666	422, 683	734.5	1.69	1.92	-5.31	-3.39	93.5	1.80

The CV measurement of all polymers in thin films was used to evaluate their electronic energy levels (highest occupied molecular orbital (HOMO) and lowest unoccupied molecular orbital (LUMO)). Figure 4c shows that all polymers displayed strong quasi-reversible oxidation peaks accompanied by irreversible reduction ones, indicating their *p*-type dominant character (*vide infra*).[40, 41] Based on oxidation and reduction onset potentials against the Fc/Fc^+ standard (− 4.8 eV), the calculated HOMO/LUMO levels of P1, P2, P3, and P4 are − 4.93/−3.26, − 5.17/−3.35, − 5.20/−3.38, and − 5.31/−3.39 eV, respectively (Table 1). As schematically visualized in their energy level diagram in Fig. 4d, the IDT donor-containing polymers (P2, P3, and P4) showed similar, deeper-lying LUMO levels compared to exclusive CDT donor-based P1 as well as gradual push-down HOMO levels with higher IDT content within the polymer repeating unit. Notably, the considerably higher-lying HOMO of P1 over the other polymers is attributed to the stronger electron-donating ability of CDT over IDT, which is in good agreement with the optical and electrochemical properties of CDT vs. IDT described above.

The DFT calculations of dimers of each polymer were modeled using the B3LYP/6-31G* basis set, with the long side chains replaced with methyl groups to reduce computation time (Figs. 5, S1, S2, **Table S2**). In addition to a similar trend of HOMO/LUMO levels with CV-derived data, for all cases, the LUMOs are centralized on electron deficient FBT units; however, the HOMOs are well-delocalized on molecular backbones. In the side view, it is observed that all dimers adopt almost coplanar backbones in the minimum-energy configuration most likely owing to noncovalent F···S and N···H intramolecular interactions within regular, alternating patterns between donor (CDT and/or IDT) and acceptor (FBT) units.[36, 42] Further, the different conformation (syn (CDT) vs. anti (IDT)) of the S-atoms of thiophenes within the donor building blocks favors different optimized ground-state structures. For example, the P1 dimer can be described as a bent, banana-type structure; both P2 and P3 dimers adopt a sigmoid-like shape, whereas P4 forms a rather linear geometry. This observation suggests that P4 has a lower degree of energetic disorder compared to others.[27, 43] Such varied conformations can significantly impact the magnitude and direction of dipole moments of dimer models, as summarized in **Figure S2** and **Table S2**. Note that relative to the models simulated for IDT-containing polymers, the P1 dimer has an overall higher dipole moment, which may increase the dipole–dipole interaction for better polymer chain assembly in the solid state.[44, 45]

Thin-Film Microstructure Analysis

Tapping-mode atomic force microscopy (AFM) was used to investigate the surface morphology of polymer films (Figs. 6a–d). To accurately compare the morphology with transistor characteristics, we passivated silicon dioxide (SiO_2) surfaces with *n*-decyltrichlorosilane (*n*-DTS) as a self-assembled monolayer before casting polymer solutions, which is described in detail in the experimental procedure. In addition, thin films were spin cast from chlorobenzene (CB) solution and annealed at each optimal temperature determined from the following FET tests. All films annealed at each optimal temperature reveal overall uniform and smooth surfaces with root mean square (RMS) values below 1.0 nm. Notably, the P1 film forms a more pronounced fibrillar microstructural feature with a relatively larger RMS (0.99 nm) compared to other films (0.31–0.39 nm), evidencing its high-order bulk organization structure, at least on the surface.[46] We further characterized the molecular orientation and crystallinity in the optimally annealed films using grazing-incidence wide angle X-ray scattering (GIWAXS) analysis. Figures 6e–l show the 2D GIWAXS patterns and corresponding line cut profiles; the relevant data are listed in **Table S3**.

The P1 polymer shows distinct long-range ordered (*n00*) lamellar diffraction peaks in the out-of-plane (OOP) and (*010*) π–π interchain diffraction peak in the in-plane (IP) direction ($d_{(100)}$ = 24.0 Å and $d_{(010)}$ = 3.57 Å), which suggests the highly crystalline microstructure (so-called crystalline polymer) with a clear edge-on dominant packing orientation. In addition, compared to IDT donor-containing polymers (CCL_{100} = 8.83–13.6 nm and CCL_{010} = 1.51–1.65 nm), P1 has larger lamellar and π–π stacking crystallite coherence lengths (CCL_{100} = 26.8 nm and CCL_{010} = 5.1 nm), as determined by the Scherrer equation, which is indicative of the formation of larger crystallites in P1. Thus, we anticipate that P1 is typically favorable for efficient charge transport through the lateral charge-hopping mechanism.[47–49]

However, IDT donor-containing polymers tend to adopt a face-on/edge-on coexisting bimodal texture, as confirmed by the strong (*010*) π–π peak in the OOP direction together with multiple (*n00*) lamellar peaks, which correspond to $d_{(010)}$ = 4.06–4.08 Å and $d_{(100)}$ = 24.0–24.2 Å, respectively. In particular, note that the ring-like halos surrounding the (*010*) π–π peak, as previously observed in other reported polymers employing an IDT unit, clearly appeared in IDT donor-containing polymers, which indicates their near-amorphous microstructure.[2, 25, 29, 33]

In addition, changes occur in the diffraction patterns among IDT donor-containing polymers. For example, both P2 and P3 possess (*100*) and (*200*) peaks in the IP direction ($d_{(100)}$ = 24.4–24.5 Å), whereas P4 shows a clear presence of multi-ordered (*00 l*) diffraction peaks along the IP direction ($d_{(001)}$ = 16.0 Å and CCL_{001} = 15.3 nm) rather than lamellar ones. Such multi-ordered (*00 l*) peaks are indicative of significant ordering along the backbone direction induced by the planarity, possibly acting to yield a strong ICT character as a positive effect on the charge transport property; this is corroborated by a series of previous studies on the amorphous IDT-BT polymer.[2]

Electrical Characterization

To evaluate the electrical properties of the polymers, two types of FET geometries, *i.e.*, bottom-gate/top-contact (BGTC) and bottom-gate/bottom-contact (BGBC), were fabricated and characterized, wherein Au was used as source and drain contact electrodes. Both device architectures are schematically shown in Fig. 7a. The devices were subjected to the thermal annealing process ranging from 180 °C to 240 °C, which showed the optimal device performance at different annealing temperatures for each polymer, *e.g.*, P1 (240 °C), P2 (180 °C), P3 (180 °C), and P4 (200 °C). Figure 7b and **Figures S3–S4** show a representative transfer and output characteristics of the best-performing FETs fabricated with the polymers, and detailed FET parameters are summarized in Table 2. Additional details of the FETs examined herein are included in the Supplementary Information. All FETs show conventional characteristics of *p*-type transistors with low threshold voltages (V_T) and high on–off ratios. For BGTC FETs with Au, P4 produced the maximum hole mobility as high as 2.22 $cm^2 V^{-1} s^{-1}$, which was approximately 4–10 times higher than those of other polymers (0.22 ~ 0.60 $cm^2 V^{-1} s^{-1}$).

MoO_3 hole injection and/or the electron blocking layer is required to produce ideal (*i.e.*, gate-bias (V_{GS})-independent) transistor characteristics with small hysteresis. Therefore, we also screened the BGTC-type FET performance by utilizing MoO_3 interfacial layers. Figure 7c shows that FETs with MoO_3 showed nearly ideal transistor characteristics with mobility values that are relatively constant over the entire V_{GS} region, presumably owing to reduced contact resistance of MoO_3/Au devices. Figure 7d and **Figures S5–S6** show contact resistance values of the P4 device at various V_{GS} extracted by the transfer-line method.[50] P4 was chosen as the transporting layer material owing to the lowest HOMO energy. The FET with MoO_3/Au yielded a relatively lower contact resistance compared to those of FET with Au electrodes over the entire V_{GS} range (− 20 to − 60 V). Notably, compared to FET with Au, FETs with MoO_3 showed somewhat reduced electrical properties similar to the trend observed in the polymer film series (Table 2). The observed highest mobility of P4 is attributed to reduced trap densities of P4 thin films. To compare trap densities of the polymers, we calculated deep trap densities (N_{tr}) from subthreshold swings (S) of BGTC FETs with MoO_3/Au using the following equation,[6]

$$N_{tr} = \frac{C_i}{e^2}\left(\frac{eS}{kT\ln 10} - 1\right), \qquad (1)$$

where C_i is the capacitance of the gate dielectric per unit area, e is the elementary charge, k is the Boltzmann constant, and T is the measured temperature. **Table S4** shows that the estimated N_{tr} value of P4 was $8.64 \cdot 10^{11}$ eV^{-1} cm^{-2}, which is smaller than those of other polymers, $(1.36–1.92) \cdot 10^{12}$ eV^{-1} cm^{-2}. Such reduced deep trap density of P4 corroborates the DFT results that P4 has the lower degree of energetic disorders than other polymers.

However, BGBC FET with Ni/Au electrodes for the polymer family performed better than BGTC FET ones for the corresponding polymers. Specifically, in BGBC FETs, hole mobilities were as high as 0.47 $cm^2 V^{-1} s^{-1}$ for P1, 0.49 $cm^2 V^{-1} s^{-1}$ for P2, 1.13 $cm^2 V^{-1} s^{-1}$ for P3, and 4.13 $cm^2 V^{-1} s^{-1}$ for P4 (**Table 2** and

Figure S7). Performance dependence on device geometry is most likely due to the morphological change between bulk and surface regions of polymer films. A similar phenomenon has also been observed in our previous study on thienoisoindigo–naphthalene polymer.[12] However, we cannot rule out the influence of Ni/Au source/drain contact resistance on the electrical property of the BGBC structure.

Driven by the significantly improved performance of the BGBC structure, we further characterized the FET properties of polymers by varying the channel length from 20 to 200 μm. (**Figure S8**) We determined that the mobilities of IDT donor-containing polymers (P2, P3, and P4) increased with longer channel length, whereas P1 showed nearly constant mobility values regardless of the channel length (**Table 2** and **Table S5**). Because IDT donor-containing polymers have deeper-lying HOMOs than P1, their mobility enhancement is partially due to the decreased portion of contact resistance in the total resistance of long-channel FETs. In addition, we determined that P4-based devices with varied channel lengths outperformed other devices, as has been observed in the abovementioned studies. Notably, an unprecedented mobility of up to 13.82 $cm^2 V^{-1} s^{-1}$ is achieved for P4-based BGBC FET at the channel length of 200 μm (**Figure 7**e and **Table 2**). Thus far, this mobility is the highest value among amorphous polymers reported in the literature and is approximately comparable to the values obtained from the recently reported highly ordered crystalline polymers. Assuming that the highest mobility can be obtained with minimized contact resistance, this result implies that P4 can produce hole mobility that is higher than the current highest value reported herein (*i.e.*, 13.82 $cm^2 V^{-1} s^{-1}$) when ohmic contacts are favorably formed at semiconductor/contact interfaces. We anticipate that interfacial doping of the semiconducting polymer area adjacent to contact electrodes is a promising approach to obtain high mobility of short-channel IDT-based FETs.[51] These results open up possibilities for achieving high mobility of IDT-based polymers by forming optimal contact junctions in FET configurations.

Stretchability

To demonstrate a certain unique feature, which originates from amorphous IDT-containing polymers over semicrystalline P1, we performed crack onset strain measurements for all polymer thin films. First, the polymer thin films were spin-cast onto SiO_2 substrates and then transferred to PDMS substrates (approximately 500-μm thickness). The polymer/PDMS films were stretched at discrete strain values (ε = 30%, 60%, and 100%) and then monitored under strain via optical microscopy. **Figure 8** shows optical microscope images of annealed polymer thin films at each strain value. Pristine (ε = 0%) P1 shows a rough, nonuniform surface with some gross aggregation, most likely due to its high crystalline nature. Numerous microcracks begin to form even at ε = 30%. However, pristine IDT-containing polymers appear to be featureless with a uniform surface and exhibit highly ductile behavior during stretching tests. Both P3 and P4 did not exhibit diamond-shaped cracks at ε = 60% strain, particularly for P3 with mechanical robustness up to ε = 100%. Although further investigation is required to understand reasons for the highest ductility of P3, we attributed such high stretchability to the amorphous nature of IDT-based polymers and more entangled IDT polymer chains. Notably, upon relaxation after being stretched at ε =

30% and 60%, amorphous IDT donor-containing polymers exhibit a wrinkled surface; in contrast, the P1 film does not exhibit wrinkles but contains chunked lumps to some extent (**Figure S9**).

In summary, we designed and synthesized four regioregular donor–acceptor polymers (P1, P2, P3, and P4) based on axisymmetric CDT and centrosymmetric IDT donors with the precise orientation of the asymmetric FBT counterpart acceptor relative to the backbone vector. The different backbone composition with the same regioregularity modifies photophysical and electrochemical properties and electronic structure of the polymers. Relative to the exclusive CDT donor-containing semicrystalline P1, IDT donor-containing amorphous polymers (P2, P3, and P4) exhibit higher hole mobilities in different FET configurations tested herein, despite their lower degree of structural order within the films, as indicated by the GIWAXS characterization. Specifically, P4-based BGBC FET reached an unprecedented value up to 13.82 $cm^2 V^{-1} s^{-1}$ at the channel length of 200 μm; this value was approximately comparable to the values obtained from recently reported highly ordered top-performing crystalline polymers. Moreover, amorphous IDT donor-containing polymer films exhibit superior deformability and ductility, particularly for P3 that has a stretchabilty up to ε = 100%. The systematic study described herein reinforces the current understanding of the structure–property relationship in terms of backbone symmetricity, composition, and regioregularity; in addition, this study upgrades the FET performance level of sporadically reported amorphous polymers, which can facilitate the rational designing of top-performing polymers for stretchable electronics applications.

Declarations

Acknowledgements

This work was supported by the National Research Foundation of Korea (NRF) grant funded by the Korea government (MSIP) (2018R1A2A1A05077194), Center for Advanced Soft-Electronics funded by the Ministry of Science and ICT as Global Frontier Project (2012M3A6A5055225), Wearable platform Materials Technology Center (2016R1A5A1009926) funded by the Korean Government (MSIT), the Research Project Funded by Ulsan City (1.200042) of UNIST (Ulsan National Institute of Science & Technology), and the National Research Foundation of Korea (NRF) grant funded by the Ministry of Science and ICT (NRF-2019R1C1C1010426 & NRF-2019M3C1B8090804).

Author Contributions

Y. C. and S. P. contributed equally. C. Y. and B. H. L conceptualized the project. Y. C. symthesized and characterized materials, as well as analyzed the data. S. P. and H. Y. carried out the device fabrication and measurement. S. J. measured UV and CV. B. L. and S. M. performed DFT calculation. Y. C. and C. Y. wrote the manuscript.

Competing financial interests:

The authors declare no competing interests.

Data availability.

The authors declare that the data supporting the findings of this study are available within the article and its Supplementary Information Files.

References

1. Cho Y, *et al.* Understanding of Fluorination Dependence on Electron Mobility and Stability of Naphthalenediimide-Based Polymer Transistors in Environment with 100% Relative Humidity. *ACS Appl Mater Interfaces* **11**, 40347–40357 (2019).
2. Zhang X, *et al.* Molecular origin of high field-effect mobility in an indacenodithiophene-benzothiadiazole copolymer. *Nat Commun* **4**, 2238 (2013).
3. Zheng Y, *et al.* An Intrinsically Stretchable High-Performance Polymer Semiconductor with Low Crystallinity. *Adv Funct Mater* **29**, 1905340 (2019).
4. Yan H, *et al.* A high-mobility electron-transporting polymer for printed transistors. *Nature* **457**, 679–687 (2009).
5. Wang W, *et al.* High-efficiency synthesis of a naphthalene-diimide-based conjugated polymer using continuous flow technology for organic field-effect transistors. *J Mater Chem C* **7**, 8450–8456 (2019).
6. Fei Z, *et al.* Alkylated Selenophene-Based Ladder-Type Monomers via a Facile Route for High-Performance Thin-Film Transistor Applications. *J Am Chem Soc* **139**, 8552–8561 (2017).
7. Dong H, Fu X, Liu J, Wang Z, Hu W. 25th Anniversary Article: Key Points for High-Mobility Organic Field-Effect Transistors. *Adv Mater* **25**, 6158–6183 (2013).
8. Ji Y, *et al.* Asymmetric Diketopyrrolopyrrole Conjugated Polymers for Field-Effect Transistors and Polymer Solar Cells Processed from a Nonchlorinated Solvent. *Adv Mater* **28**, 943–950 (2016).
9. Back JY, *et al.* Investigation of Structure–Property Relationships in Diketopyrrolopyrrole-Based Polymer Semiconductors via Side-Chain Engineering. *Chem Mater* **27**, 1732–1739 (2015).
10. Yao J, *et al.* Significant Improvement of Semiconducting Performance of the Diketopyrrolopyrrole-Quaterthiophene Conjugated Polymer through Side-Chain Engineering via Hydrogen-Bonding. *J Am Chem Soc* **138**, 173–185 (2016).
11. Yu Y, *et al.* Effect of conjugation length on the properties of fused perylene diimides with variable isoindigos. *J Mater Chem C* **7**, 12263–12269 (2019).
12. Kim G, *et al.* A Thienoisoindigo-Naphthalene Polymer with Ultrahigh Mobility of 14.4 cm2/V·s That Substantially Exceeds Benchmark Values for Amorphous Silicon Semiconductors. *J Am Chem Soc* **136**, 9477–9483 (2014).

13. Zhang A, *et al.* Effect of Fluorination on Molecular Orientation of Conjugated Polymers in High Performance Field-Effect Transistors. *Macromolecules* **49**, 6431–6438 (2016).
14. Wang M, Ford MJ, Lill AT, Phan H, Nguyen TQ, Bazan GC. Hole Mobility and Electron Injection Properties of D-A Conjugated Copolymers with Fluorinated Phenylene Acceptor Units. *Adv Mater* **29**, 1603830 (2017).
15. Huang C-F, *et al.* Packing Principles for Donor–Acceptor Oligomers from Analysis of Single Crystals. *Chem Mater* **28**, 5175–5190 (2016).
16. Ying L, *et al.* Regioregular pyridal[2,1,3]thiadiazole pi-conjugated copolymers. *J Am Chem Soc* **133**, 18538–18541 (2011).
17. Cho Y, *et al.* Guest-oriented non-fullerene acceptors for ternary organic solar cells with over 16.0% and 22.7% efficiencies under one-sun and indoor light. *Nano Energy* **75**, 104896 (2020).
18. Wu W, Liu Y, Zhu D. Pi-conjugated molecules with fused rings for organic field-effect transistors: design, synthesis and applications. *Chem Soc Rev* **39**, 1489–1502 (2010).
19. Yum S, *et al.* Benzotriazole-Containing Planar Conjugated Polymers with Noncovalent Conformational Locks for Thermally Stable and Efficient Polymer Field-Effect Transistors. *Chem Mater* **26**, 2147–2154 (2014).
20. Onwubiko A, *et al.* Fused electron deficient semiconducting polymers for air stable electron transport. *Nat Commun* **9**, 416 (2018).
21. Kim U, *et al.* Zwitterionic Conjugated Surfactant Functionalization of Graphene with pH-Independent Dispersibility: An Efficient Electron Mediator for the Oxygen Evolution Reaction in Acidic Media. *Small* **16**, 1906635 (2020).
22. Cho Y, *et al.* Dithienogermole-Based Nonfullerene Acceptors: Roles of the Side-Chains' Direction and Development of Green-Tinted Efficient Semitransparent Organic Solar Cells. *ACS Applied Energy Materials*, (2020).
23. Wang M, Ford M, Phan H, Coughlin J, Nguyen T-Q, Bazan GC. Fluorine substitution influence on benzo[2,1,3]thiadiazole based polymers for field-effect transistor applications. *Chem Commun* **52**, 3207–3210 (2016).
24. Ying L, Huang F, Bazan GC. Regioregular narrow-bandgap-conjugated polymers for plastic electronics. *Nat Commun* **8**, 14047 (2017).
25. Wadsworth A, *et al.* Modification of Indacenodithiophene-Based Polymers and Its Impact on Charge Carrier Mobility in Organic Thin-Film Transistors. *J Am Chem Soc* **142**, 652–664 (2020).
26. Li Y, Tatum WK, Onorato JW, Zhang Y, Luscombe CK. Low Elastic Modulus and High Charge Mobility of Low-Crystallinity Indacenodithiophene-Based Semiconducting Polymers for Potential Applications in Stretchable Electronics. *Macromolecules* **51**, 6352–6358 (2018).
27. Venkateshvaran D, *et al.* Approaching disorder-free transport in high-mobility conjugated polymers. *Nature* **515**, 384–388 (2014).

28. Li Y, Tatum WK, Onorato JW, Barajas SD, Yang YY, Luscombe CK. An indacenodithiophene-based semiconducting polymer with high ductility for stretchable organic electronics. *Polym Chem* **8**, 5185–5193 (2017).
29. Zhong W, *et al.* High-Performance Organic Field-Effect Transistors Fabricated Based on a Novel Ternary pi-Conjugated Copolymer. *ACS Appl Mater Interfaces* **9**, 7315–7321 (2017).
30. Lee J, *et al.* An Ultrahigh Mobility in Isomorphic Fluorobenzo[c][1,2,5]thiadiazole-Based Polymers. *Angew Chem Int Ed Engl* **57**, 13629–13634 (2018).
31. Wang M, Ford MJ, Zhou C, Seifrid M, Nguyen TQ, Bazan GC. Linear Conjugated Polymer Backbones Improve Alignment in Nanogroove-Assisted Organic Field-Effect Transistors. *J Am Chem Soc* **139**, 17624–17631 (2017).
32. Planells M, *et al.* The effect of thiadiazole out-backbone displacement in indacenodithiophene semiconductor polymers. *J Mater Chem C* **2**, 8789–8795 (2014).
33. Zhang W, *et al.* Indacenodithiophene Semiconducting Polymers for High-Performance, Air-Stable Transistors. *J Am Chem Soc* **132**, 11437–11439 (2010).
34. Madathil PK, Cho S, Choi S, Kim T-D, Lee K-S. Synthesis and Characterization of Cyclopentadithiophene and Thienothiophene-Based Polymers for Organic Thin-Film Transistors and Solar Cells. *Macromol Res* **26**, 934–941 (2018).
35. Li C-H, Kettle J, Horie M. Cyclopentadithiophene–naphthalenediimide polymers; synthesis, characterisation, and n-type semiconducting properties in field-effect transistors and photovoltaic devices. *Mater Chem Phys* **144**, 519–528 (2014).
36. Casey A, Han Y, Fei Z, White AJP, Anthopoulos TD, Heeney M. Cyano substituted benzothiadiazole: a novel acceptor inducing n-type behaviour in conjugated polymers. *J Mater Chem C* **3**, 265–275 (2015).
37. Zhou H, Yang L, You W. Rational Design of High Performance Conjugated Polymers for Organic Solar Cells. *Macromolecules* **45**, 607–632 (2012).
38. Wang C, Ouyang L, Xu X, Braun S, Liu X, Fahlman M. Relationship of Ionization Potential and Oxidation Potential of Organic Semiconductor Films Used in Photovoltaics. *Sol RRL* **2**, 1800122 (2018).
39. Ma Y-S, *et al.* Perylene Diimide Dyes Aggregates: Optical Properties and Packing Behavior in Solution and Solid State. *Supramolecular Chemistry* **19**, 141–149 (2007).
40. Sirringhaus H. 25th Anniversary Article: Organic Field-Effect Transistors: The Path Beyond Amorphous Silicon. *Adv Mater* **26**, 1319–1335 (2014).
41. Mishra A, Bauerle P. Small molecule organic semiconductors on the move: promises for future solar energy technology. *Angew Chem Int Ed Engl* **51**, 2020–2067 (2012).
42. Raychev D, Guskova O, Seifert G, Sommer J-U. Conformational and electronic properties of small benzothiadiazole-cored oligomers with aryl flanking units: Thiophene versus Furan. *Computational Materials Science* **126**, 287–298 (2017).

43. Suzuki F, Kubo S, Fukushima T, Kaji H. Effects of Structural and Energetic Disorders on Charge Transports in Crystal and Amorphous Organic Layers. *Sci Rep* **8**, 5203 (2018).
44. Yun JH, *et al.* Enhancement of charge transport properties of small molecule semiconductors by controlling fluorine substitution and effects on photovoltaic properties of organic solar cells and perovskite solar cells. *Chem Sci* **7**, 6649–6661 (2016).
45. Borsenberger PM, Fitzgerald JJ. Effects of the dipole moment on charge transport in disordered molecular solids. *J Phys Chem* **97**, 4815–4819 (1993).
46. Wang Z-Y, *et al.* Precise tracking and modulating aggregation structures of conjugated copolymers in solutions. *Polym Chem* **11**, 3716–3722 (2020).
47. Nguyen TL, *et al.* Ethanol-Processable, Highly Crystalline Conjugated Polymers for Eco-Friendly Fabrication of Organic Transistors and Solar Cells. *Macromolecules* **50**, 4415–4424 (2017).
48. McCulloch I, *et al.* Liquid-crystalline semiconducting polymers with high charge-carrier mobility. *Nat Mater* **5**, 328–333 (2006).
49. Sirringhaus H, *et al.* Two-dimensional charge transport in self-organized, high-mobility conjugated polymers. *Nature* **401**, 685–688 (1999).
50. Choi S, *et al.* A Study on Reducing Contact Resistance in Solution-Processed Organic Field-Effect Transistors. *ACS Appl Mater Interfaces* **8**, 24744–24752 (2016).
51. Xu Y, Sun H, Shin EY, Lin YF, Li W, Noh YY. Planar-Processed Polymer Transistors. *Adv Mater* **28**, 8531–8537 (2016).

Tables And Schemes

Due to technical limitations, full-text HTML conversion of Scheme 1 and Table 2 could not be completed. However, they can be accessed in the Supplementary Files.

Figures

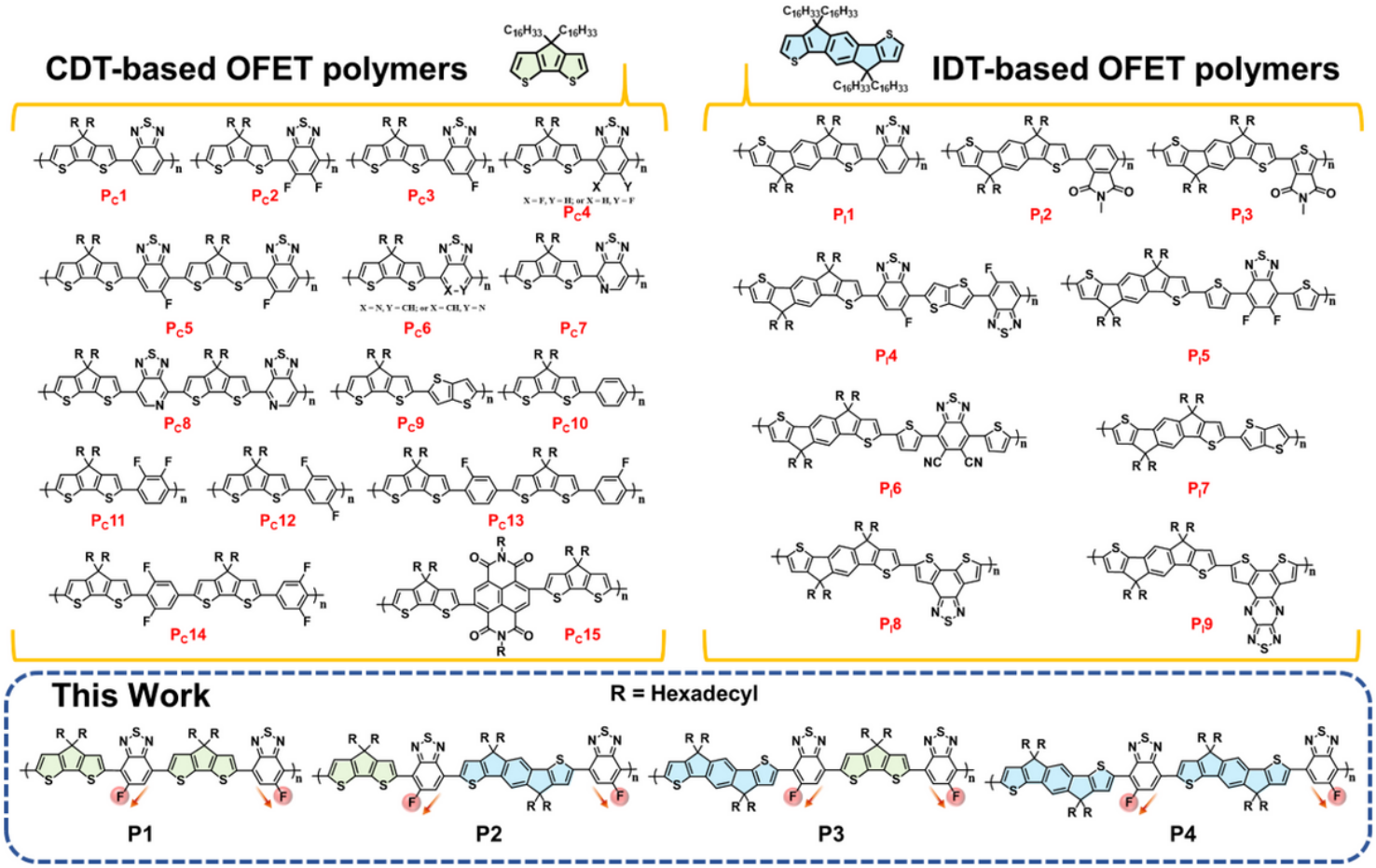

Figure 1

Chemical structures of CDT- and IDT-based OFET polymers reported in the literatures and this work.

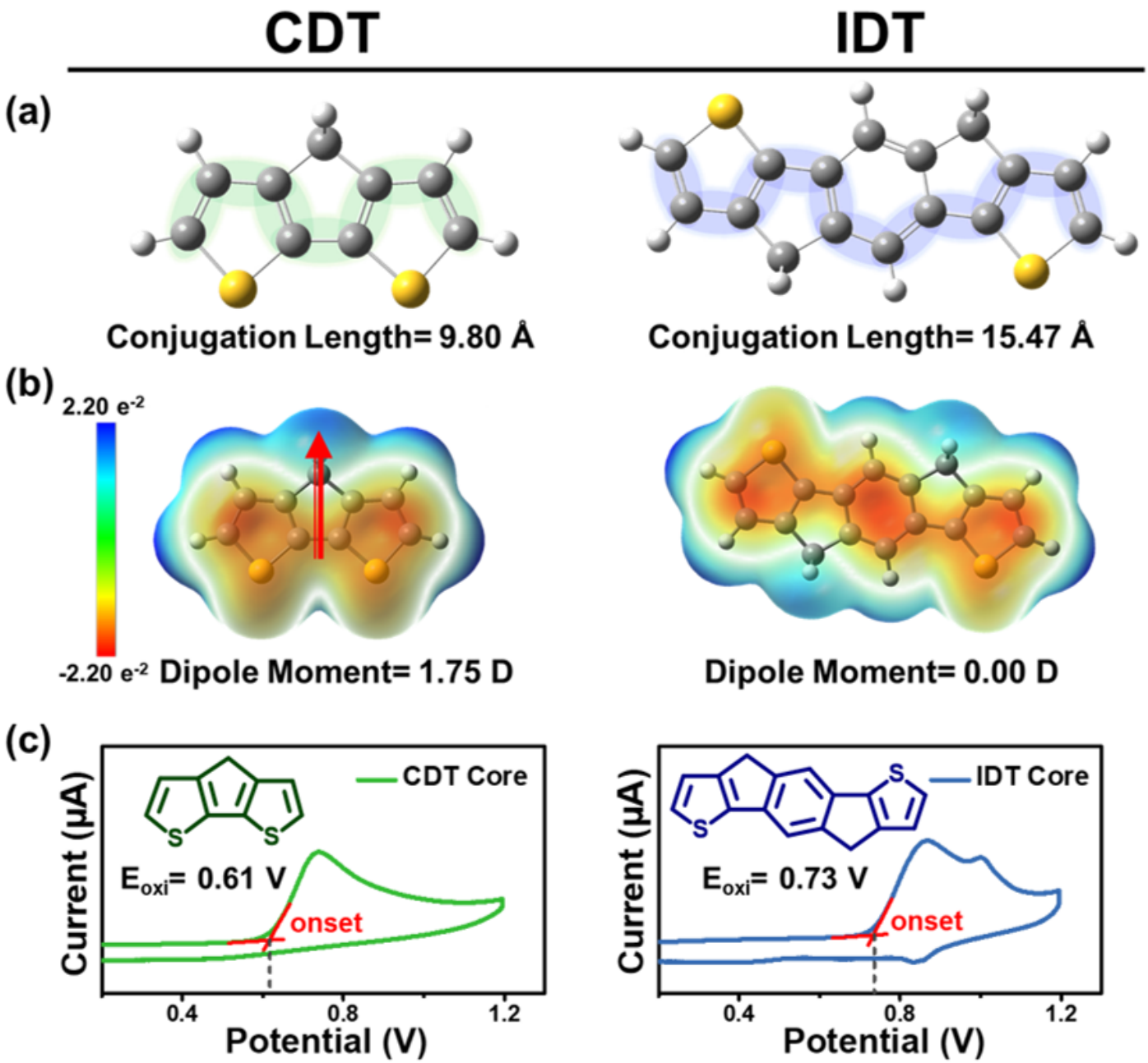

Figure 2

Comparison of CDT and IDT core units. DFT-calculated (a) optimized geometries with conjugation length, (b) electrostatic potential, and (c) CV-derived oxidation potential of CDT and IDT cores.

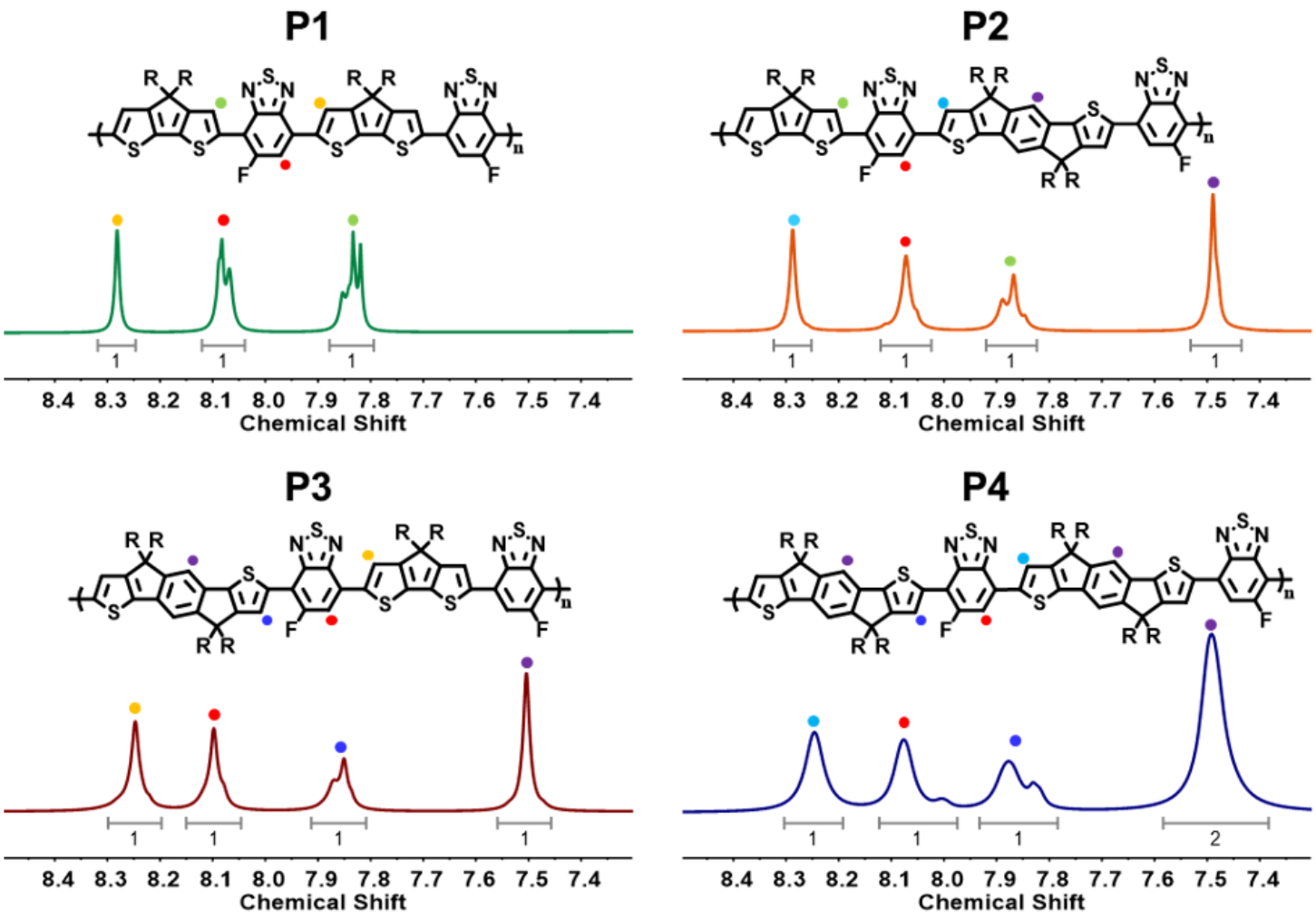

Figure 3

1H NMR spectra of the polymers.

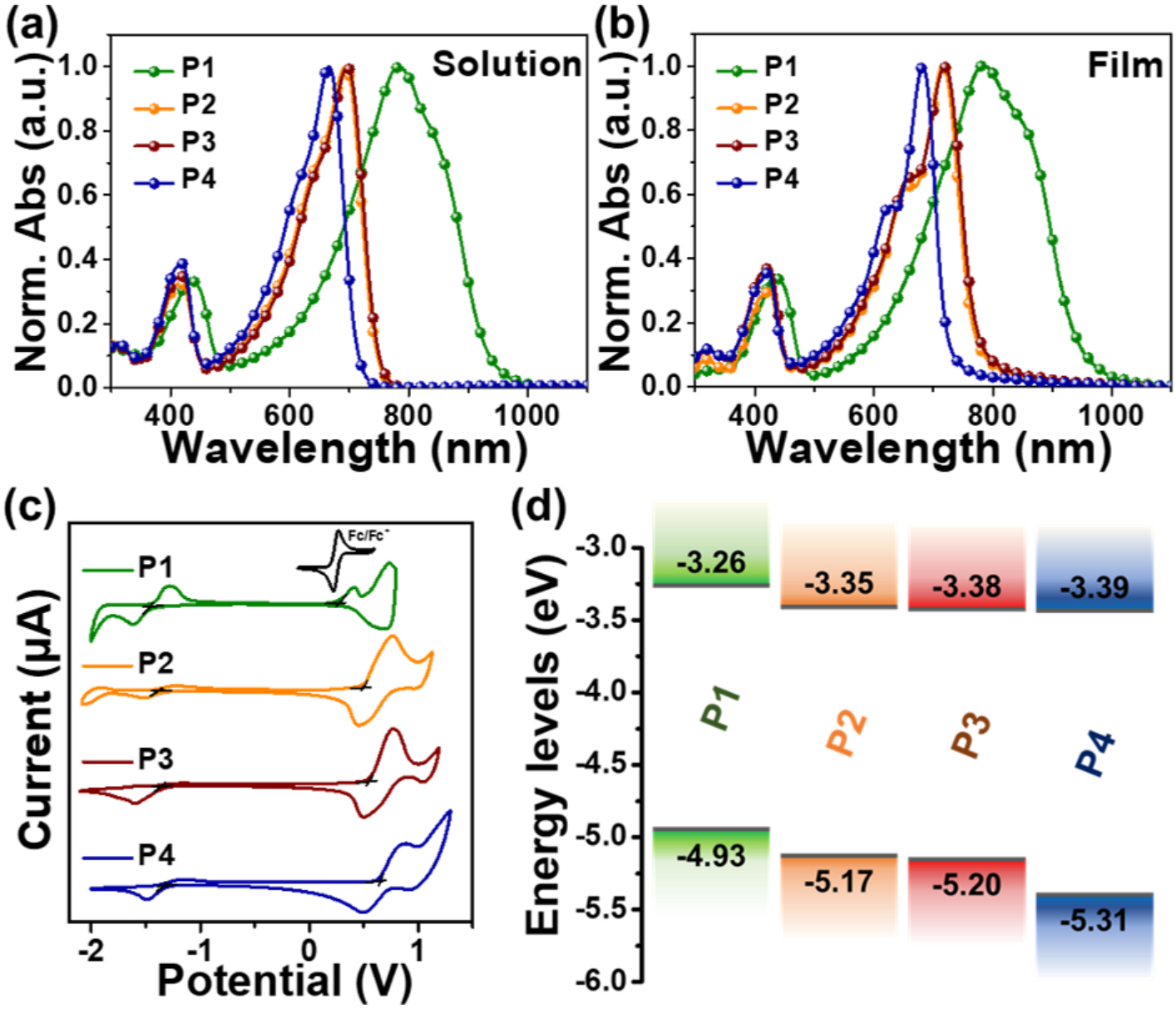

Figure 4

Optoelectrical properties of polymers. Normalized UV-vis-NIR absorption spectra in (a) thin film and (b) CF solution, (c) CV, and (d) energy level diagram of the polymers.

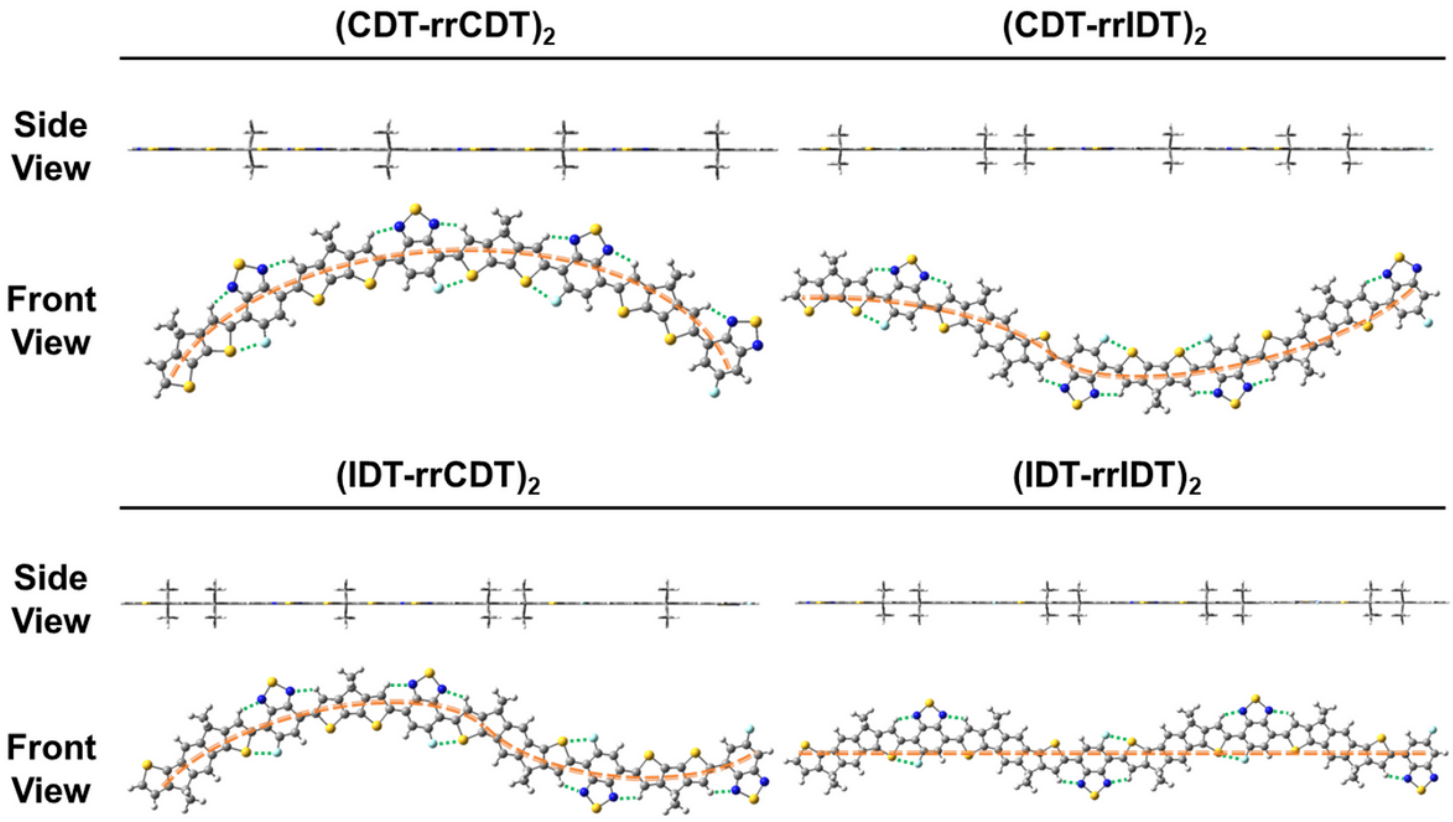

Figure 5

Optimized geometries of dimers by DFT calculation.

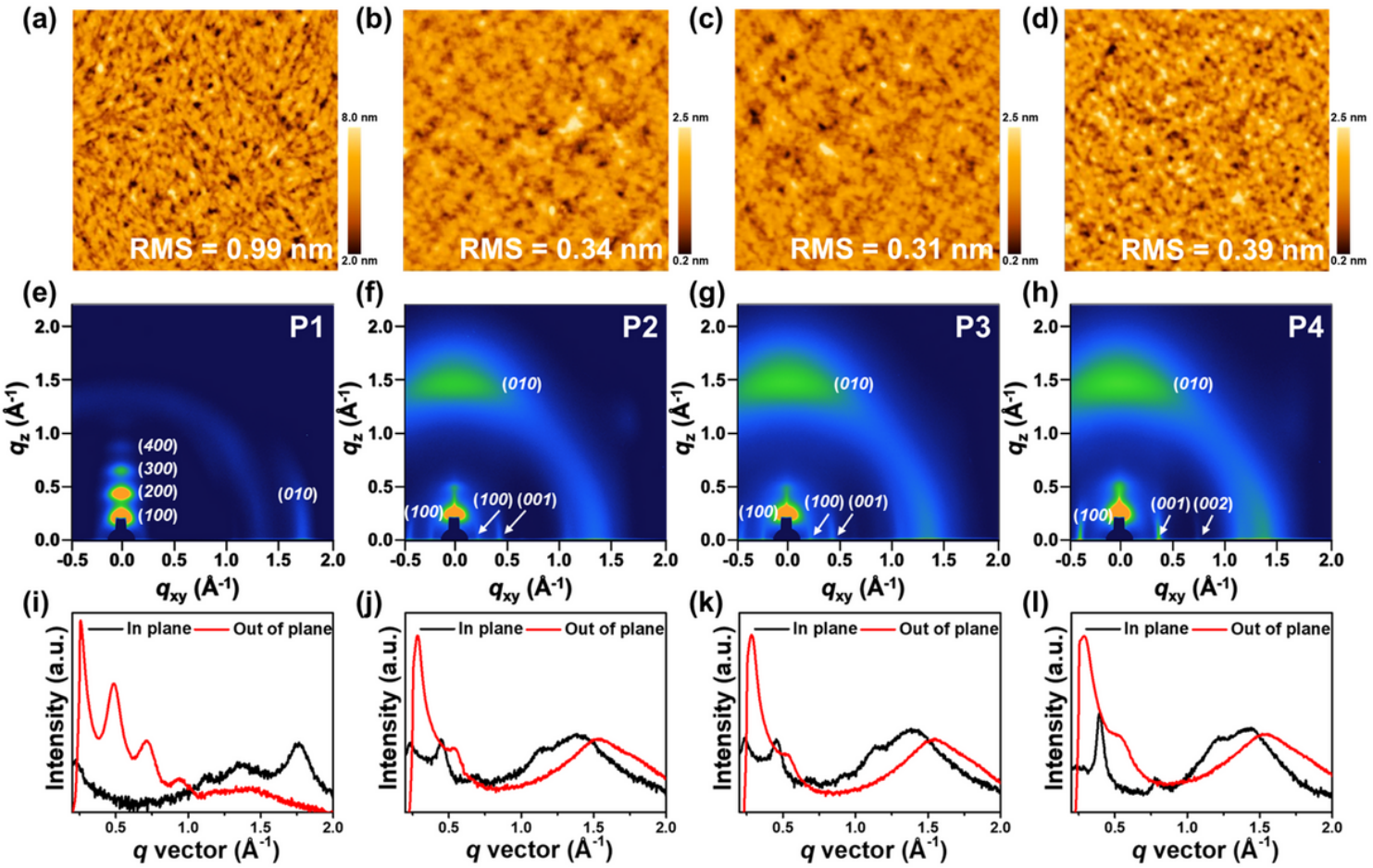

Figure 6

Morphologies and crystalline properties of polymers. 2 μm × 2 μm scaled AFM topographic images of (a) P1, (b) P2, (c) P3, and (d) P4 films annealed under optimized temperatures. The 2D GIWAXS pictures (e-h) and the line cut profiles (i-l) of the P1 (e and i), P2 (f and j), P3 (g and k), and P4 (h and l) films annealed under optimized temperatures.

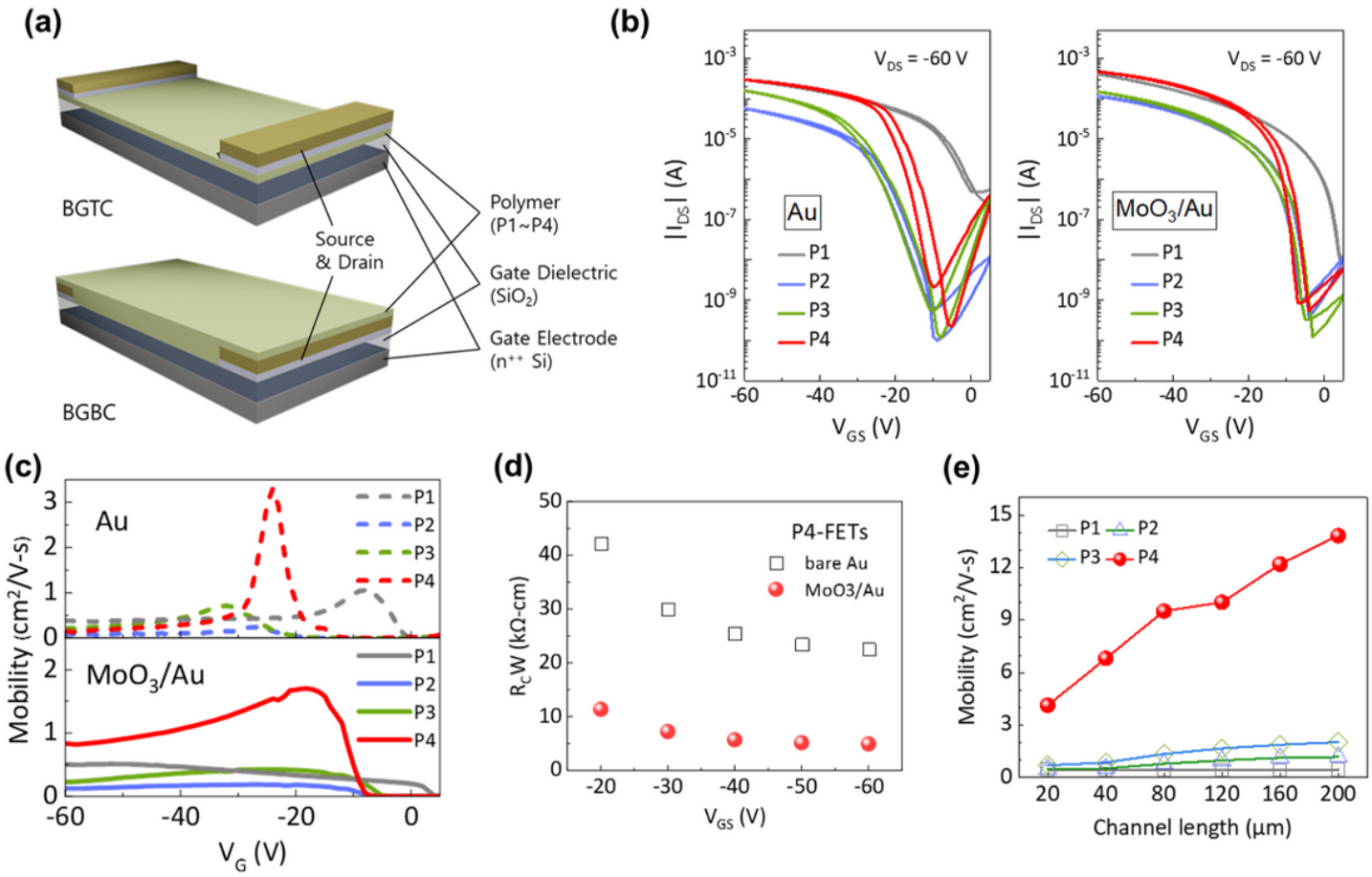

Figure 7

FET characteristics. (a) Schematic architecture of BGTC and BGBC FETs, (b) transfer characteristics of the BGTC devices (Au or MoO3/Au source and drain electrodes) annealed at optimal temperatures of 240 oC (for P1), 180 oC (for P2 and P3), and 200 oC (for P4), (c) mobility variation of the polymers, (d) channel width-normalized contact resistance of the P4 FETs with or without a MoO3 interfacial layer as a function of gate voltages, and (e) mobility variation of the BGBC devices with Ni/Au as a function of channel lengths.

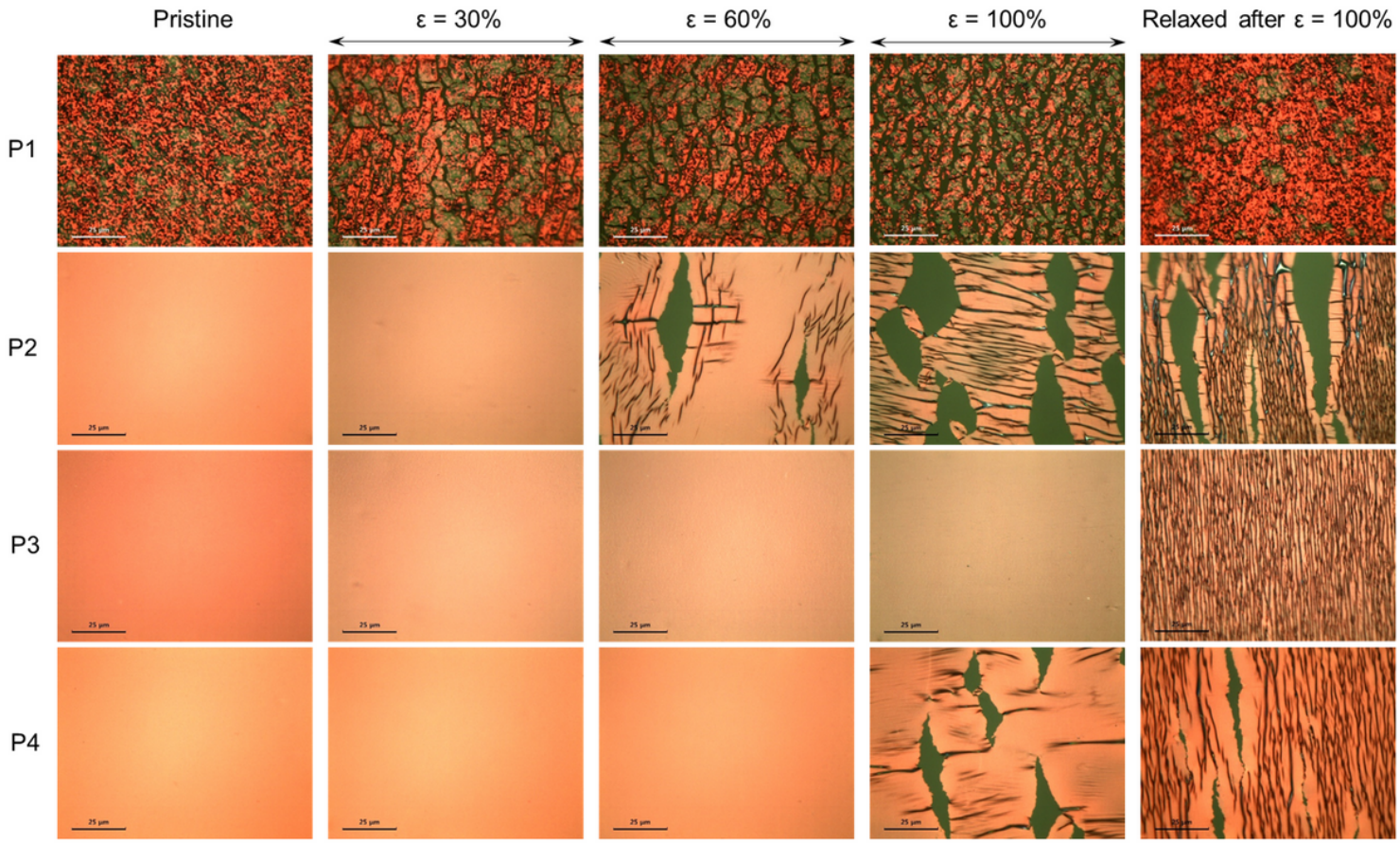

Figure 8

Optical microscopic images of the polymer/PDMS films with varying stain values (0 - 100%). The arrows indicate direction parallel to stretching of the films. The scale bars are 25 μm.

Supplementary Files

This is a list of supplementary files associated with this preprint. Click to download.

- Scheme1.png
- Table2.docx
- SupplementaryInformation.docx